ON TWO-DIMENSIONAL MODELING OF MAGNETOTELLURIC FIELD DATA

YASUO OGAWA
Volcanic Fluid Research Center, Tokyo Institute of Technology, 2-12-1 Ookayama, Meguro, Tokyo, 152-8551, Japan, E-mail: oga@ksvo.titech.ac.jp

(Received 19 January 2001; Accepted 2 November 2001)

Abstract. In this paper, some recent topics on the modeling of magnetotelluric data are introduced. The focus is on the handling of real field data for two-dimensional resistivity modeling. First, the removal of the effects of near surface heterogeneity is reviewed. It covers telluric distortions (phase mixing and static shift) and magnetic distortions using conventional Groom-Bailey type 3D/2D model (three-dimensional local anomaly underlain by regional two-dimensional structure). The extension of a 3D/2D distortion model for multi-site, multi-frequency is a new development. Magnetic distortion seems to be less significant for land observations, but significant for sea floor data, where the regional magnetic field is weak due to seawater. In special cases involving for example, distortion due to topography and bathymetry, explicit removal is possible. There are some schemes proposed for a 3D/3D model (three-dimensional local anomaly underlain by regional three-dimensional structure). Along with the removal of the distortion, it is important to recognize the dimensionality of the dataset prior to modeling. A property using strike estimates for each site is an indicator for dimensionality which is unaffected by local distortion. Mapping the local strike or a rose diagram is an effective visualization of the dimensionality.

Two-dimensional inversion is becoming routine. For the fast calculation of derivatives, approximate calculation, reciprocity or conjugate gradient methods are used. In order to incorporate a priori information and to overcome the intrinsic ill-posed nature of the inversion problem, imposing constraints on the model structure is important. A proper tradeoff between the data fit and constraints should be optimized to obtain minimum structures that are required by the field data. However, the choice of constraints is rather subjective and depends on the geological situations. For field data, two-dimensional inversion has limits on modes, area, and period range. Special care must be taken for the structure outside the profile. Two-dimensional inversion incorporating anisotropy is interesting and becoming popular, but the structure may not be unique. Future development in three-dimensional inversion for real datasets should take the above points into consideration.

Keywords: field data, magnetotelluric theory, two-dimensional modeling

1. Introduction

In recent years, advances in magnetotelluric (MT) theory along with computer technology and equipment, have enabled detailed modeling of the Earth's conductivity distribution. In this paper, I review some topics on the modeling using MT field data. In the 1990s, broadband equipment with large dynamic range and sophisticated time series analyses (for example, Chave and Thomson, 1989; Larsen et al., 1996; Egbert, 1997) successfully provided unbiased robust impedance es-

Surveys in Geophysics **23:** 251–272, 2002.

timates for a wide period range. High precision impedance data then started to demand detailed modeling of the Earth. Modeling of real data usually includes the following steps. (1) The pre-processing of the data for near-surface heterogeneity, which is much shallower and smaller than the target structure. (2) Checking the dimensionality of the dataset. (3) Two- and three-dimensional modeling. In this paper, I present some topics on these steps.

2. Removal of Effects from Near-Surface Heterogeneity

The effect of surface heterogeneity on MT responses has been recognized since the 1970s and methods for its removal have been proposed (Berdichevsky and Dmitriev, 1976; Larsen, 1977; Bahr, 1985; Groom and Bailey, 1989; Chave and Smith, 1994; Smith 1995, 1997). It is important to identify and remove the near-surface effect prior to regional modeling.

2.1. Basic principles

First, we will investigate the perturbations of electric and magnetic field due to a small anomaly from the basic principles following Chave and Smith (1994) and Utada and Munekane (2000). Suppose we have a regional conductivity structure of σ_0, a magnetic permeability μ_0, and regional electric and magnetic fields as E_0 and H_0 for a sinusoidal angular frequency of ω. Given a conductivity anomaly $\delta\sigma$ in the volume V', the total electric field E will be given by Equation (1), by use of a Green's function g.

$$\begin{aligned} E(r) &= E_0(r) - i\omega\mu_0 \int_{V'} \mathrm{d}V' g(r, r')\delta\sigma(r')E(r') \\ &\quad + \nabla\frac{1}{\sigma_0}\nabla \cdot \int_{V'} \mathrm{d}V' g(r, r')\delta\sigma(r')E(r'). \end{aligned} \tag{1}$$

The second term on the right hand side represents the electric field due to the induction within the anomaly, whereas the third term represents the electric field due to the galvanic charge at the anomaly surface. If the anomaly is small enough and the frequency is low, the second term is negligible compared with the third. By approximating $E(r')$ as $E_0(r')$, the third term is further expressed as αE_0, where α is a frequency independent 2×2 real tensor. Then the total E field is a product of a frequency independent 2×2 real tensor C and the regional electric field as shown in Equation (2).

$$E = E_0 + \alpha E_0 = C E_0. \tag{2}$$

Regarding the magnetic field, by taking the curl of Equation (1), we have the following. (Note here the charge term in Equation (1) is dropped.)

$$H(r) = H_0(r) + \nabla \times \int_{V'} \mathrm{d}V' g(r, r')\delta\sigma(r')E(r'). \tag{3}$$

If the anomaly is small enough, the approximation of $E(r')$ as E_0 will lead to the following,

$$H = H_0 + DE_0, \tag{4}$$

where D is a frequency-independent 2×2 real tensor.

If we can assume the regional field we can estimate the distortion tensors C and D directly from electric and magnetic fields from Equations (2) and (4). However, we usually only observe the ratio of the electric field to magnetic field, i.e., the impedances. The regional and distorted impedances Z_0 and Z are defined by $E_0 = Z_0 H_0$ and $E = ZH$, respectively. Thus, using Equations (2) and (4), the distorted impedance is expressed as follows:

$$Z = CZ_0(I + DZ_0)^{-1}. \tag{5}$$

2.2. TELLURIC DISTORTIONS

For the present, let us ignore the magnetic distortion by assuming $D = 0$. Telluric distortions can be classified into the two categories. One is the distortion of the telluric orthogonality (also called phase mixing) and the other is the distortion of the telluric amplitudes (often called the static shift).

2.2.1. *Phase Mixing (Distortions of the Telluric Orthogonality)*

If the surface distortion is caused by a three-dimensional surface anomaly that overlies a two-dimensional regional structure, the Groom–Bailey (1989) decomposition technique is widely used.

The Groom–Bailey scheme decomposes the observed impedance Z_{obs} in the following way.

$$Z_{\text{obs}} = R(gTSAZ_{2d})R^{-1} \tag{6}$$

Z_{obs} and Z_{2d} are the observed and regional two-dimensional impedances, respectively. Z_{2d} has only off-diagonal components. R is the rotation matrix for conversion between the observed and the regional coordinate systems.

$$R = \begin{bmatrix} \cos\theta & \sin\theta \\ -sin\theta & \cos\theta \end{bmatrix}.$$

The angle θ is the strike direction, measured counter-clockwise from the observed coordinate system. g is a scalar called site gain. T, S, A are called the twist tensor, shear tensor and anisotropy tensor, respectively and defined as below.

$$T = \begin{bmatrix} 1 & -t \\ t & 1 \end{bmatrix}, \quad S = \begin{bmatrix} 1 & e \\ e & 1 \end{bmatrix}, \quad A = \begin{bmatrix} 1+s & 0 \\ 0 & 1-s \end{bmatrix}. \tag{7}$$

The three real parameters t, e, s are called twist, shear and anisotropy respectively. Twist and shear are descriptors for the orthogonality of the electric and magnetic fields, whereas site gain and anisotropy represent the "static shift". Equation (6) can be rewritten as follows:

$$Z_{\text{obs}} = RTSZ'_{2d}R^{-1}, \tag{8}$$

$$Z'_{2d} = gAZ_{2d}.$$

where Z'_{2d} is a static shift contaminated impedance.

From the Groom–Bailey decomposition, we can determine strike direction, twist and shear, but cannot uniquely determine site gain and anisotropy, (i.e., static shift). We can only determine Z'_{2d}, which includes static shift.

Since Groom–Bailey decomposition assumes a two-dimensional regional resistivity structure with a three-dimensional superficial anomaly, it is natural to extend the decomposition scheme for a set of sites, where we can expect a two-dimensional resistivity structure. McNeice and Jones (2001) introduced a multi-site multi-frequency decomposition scheme, where twist and shear parameters are site-dependent and frequency-independent, but the regional strike is site-independent and frequency-independent. The strike direction is the least stable parameter among the distortion parameters, if the MT data are contaminated by noise and telluric distortion (Jones and Groom, 1993). The use of a multi-site multi-frequency method has an advantage in stabilizing the estimate of the regional strike.

If we know the regional two-dimensional strike properly, the rotated impedance (without decomposition) has the following form.

$$\begin{aligned} Z^{\text{rot}}_{\text{obs}} &= R^{-1}Z_{\text{obs}}R = (TS)Z'_{2d} \\ &= \begin{pmatrix} 1-te & e-t \\ e+t & 1+te \end{pmatrix} \begin{pmatrix} 0 & Z'_{TE} \\ Z'_{TM} & 0 \end{pmatrix} \\ &= \begin{pmatrix} (e-t)Z'_{TM} & (1-te)Z'_{TE} \\ (1+te)Z'_{TM} & (e+t)Z'_{TE} \end{pmatrix}, \end{aligned} \tag{9}$$

where Z'_{2d} is defined in Equation (8). Looking at the off-diagonal impedances, the factors $(1-te)$ and $(1+te)$ are affecting the two-dimensional impedances Z'_{TE} and Z'_{TM} like static shift factors. Erroneous estimate of twist and shear will be absorbed in static shifts, if the strike is properly estimated. Equation (9) also means that if we rotate the impedance properly, we can use the off-diagonal impedance without decomposition, where twist and shear parameters will play the role of static shift.

2.2.2. *Static Shift (Distortions of the Telluric Amplitude)*

The amplitudes of regional impedances (regional apparent resistivity) remain undetermined even after the tensor decomposition. This is because the static shift (the site gain and anisotropy in Groom-Bailey terminology) cannot be solved by tensor

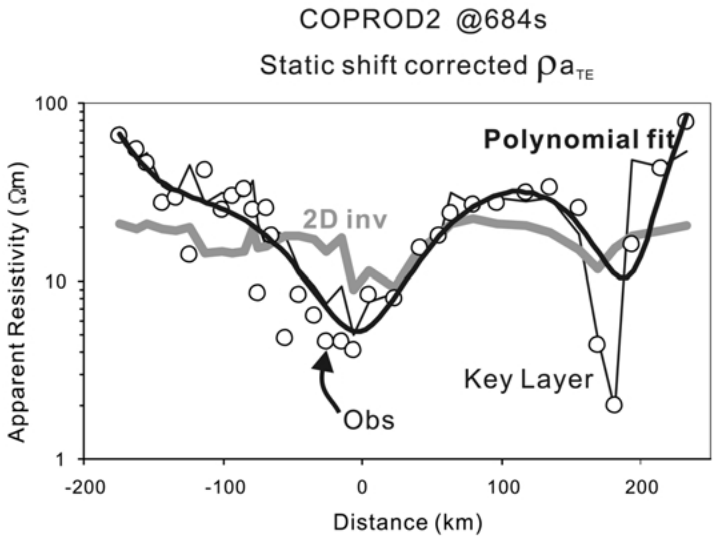

Figure 1. Comparison of static shift removal schemes for the COPROD2 dataset.

decomposition alone. There are three categories of methods to remove the static shift.

(1) The first is the spatial filtering such as EMAP method (Torres-Verdin and Bostick, 1992). In an EMAP configuration, where electric dipoles continuously cover the profile, one can spatially smooth out the static shift by low-pass filtering the electric field. A longer dipole length is used for longer period. Long dipole measurements using telephone lines also help to elucidate static shift by small-scale anomalies for mantle studies (Tounerie and Chouteau, 1998; Uyeshima et al., 2001). For conventional MT measurements, the electric dipoles are not distributed spatially continuously. Berdichevsky et al. (1980) spatially averaged the apparent resistivities (using a determinant average of impedance tensors) for each period, on the assumption that the regional structure is one-dimensional. A more flexible case is the one where the regional deep structure varies smoothly. If the regional structure is two-dimensional, we can expect that the regional (static-shift-removed) TE apparent resistivity will vary spatially smoothly for long periods (e.g., Jones et al., 1992). A thick black line in Figure 1 shows the application of this method to the COPROD2 dataset (Jones, 1993). The regional apparent resistivity at the period of 682s is given by a regression curve to the observed apparent resistivity.

(2) The second category uses other independent information that is free from galvanic distortion. Use of well-logging data is one such method. Jones (1988) used a conductive "key layer" known by well-logging and shifted apparent resistivity curves so that the local one-dimensional models have a conductor whose resistivity is the same as that of the key-layer . The depth of the key layer is not controlled. The example of this method is shown in Figure 1 for the COPROD2 dataset. A thin black line shows the regional (static shift removed) apparent resistivity distribution

from this method. The sites near 180km show large anomalously low apparent resistivity and they are interpreted as originating from regional structure. On the other hand the previous polynomial fitting does not require such a spatial sharp feature as a regional structure.

The joint use of MT and in-loop time-domain sounding is another way (Pellerin and Hohmann, 1990; Meju, 1996; Harinarayana, 1999). This method determines the shallow one-dimensional structure using the magnetic field only, which is robust against galvanic charges. However this method has to assume one-dimensionality in the shallow common depth for MT and time-domain soundings. Another control of static shift is to use the deep structure known from another method. Schultz et al. (1993) made lake bottom magnetotelluric measurements and shifted the apparent resistivity curves so that the deep structure is consistent with the known geomagnetic depth sounding data.

(3) The third is to solve the static shifts as unknown variables jointly with inversion modeling. This method is applied to two-dimensional inversion (deGroot-Hedlin, 1991; Ogawa and Uchida, 1996). deGroot-Hedlin (1991) made the assumption that the static shift must sum up to zero. Ogawa and Uchida (1996) defined the L2 norm of the static shift and inverted the resistivity model under the assumption that the L2 norm should be small. The grey line in Figure 1 shows the regional apparent resistivity for the COPROD2 dataset by a two-dimensional inversion (Ogawa and Uchida, 1996). As seen in Figure 1, three different methods for static correction do not give the same result. The results depend on the assumptions.

The introduction of a larger error for apparent resistivity compared with those for the phase is another implicit way to deal with the static shift in the inversion (Wu et al., 1993). In this case, the inversion model will primarily try to fit the observed phase, which will give fit to the shape of the apparent resistivity, whereas the large error of apparent resistivity will effectively accommodate the static shift.

These methods, which use static shift as part of model parameters, can be applied to a dataset where there are no other data available for the correction.

The static shift is caused by the surface resistivity gradient. Thus the static shift is also realized by the lateral resistivity variation for the TM mode. This means that the static shifts in TM mode and static shifts are not independent. The horizontal roughness constraint on the surface affects the static shift in TM mode. An example is shown in Ogawa (1999) for the COPROD2S2 dataset prepared by Ivan Varentsov.

2.3. MAGNETIC DISTORTION

The effect of magnetic distortion can be found at relatively short periods. It is because the DZ_0 term in Equation (5) will become smaller for longer periods. Chave and Jones (1997) demonstrated that the inclusion of magnetic distortion could improve the fit for the BC87 dataset.

For field data, we can only recognize the distortion in terms of impedances. However, for numerical modeling, we can directly compute electric and magnetic fields for both the distorted and the undistorted case. We can calculate C and D tensors directly and check if they are real and if they are significant. Agarwal and Weaver (2000) made numerical testing of a local three-dimensional anomaly over a regional two-dimensional structure. They found magnetic distortion is negligible even for reasonable cases of strong current channeling on land observation.

However, in the case of sea floor data, the situation is different. It is because the amplitude of the regional magnetic field is significantly dissipated due to the thick conductive ocean, whereas the conductive ocean can induce large distorted magnetic fields. The bathymetry will go into $\delta\sigma$ in Equation (3) and significantly contribute to the tensor D. Then, H_0 will become comparable to DE_0 in Equation (4) and DZ_0 will be comparable to I. White at al. (1997) showed that a model without magnetic distortion could not fit the observed data, and that the inclusion of a magnetic distortion parameter was essential for a better fit.

2.4. Explicit distortion modeling

If the surface inhomogeneity is known, we can directly calculate the distortion parameter in a deterministic way, and can remove the effect from the impedance tensor. This is called tensor stripping (Jiracek, 1990). Two-dimensional topographic responses were estimated by the finite element code (Wannamaker et al., 1986) or the Rayleigh-FFT method (Jiracek et al., 1989). It is noted that the TM mode has a significant effect even at long periods due to the galvanic charge at the slope. If we can assume that there is no electromagnetic coupling between the topography and the underground structure, we can explicitly correct the effect of topography. Alternatively, the topography can be included as a model structure using a finite element code and calculate the response and Frechet derivatives including both the structure and the topography (e.g., Ogawa et al., 1998).

As for seafloor applications, the effect of the conductive ocean is significant. If the ocean can be regarded as a thin layer compared with the skin depth, the explicit correction for the bathymetry is possible if the Earth structure is decoupled with the conductive ocean (Nolasco et al., 1998). In general cases, we need a good approximation of the sea floor topography and have a heavy computational load. Baba and Seama (2002) proposed efficient three-dimensional bathymetry modeling by use of a transformation of numerical grids together with magnetic permeability and electric conductivity. Figures 2 show the basic idea. The topography of the seafloor (Figure 2a) is usually realized by discretizing the slopes by meshes (Figure 2b). An accurate calculation needs fine mesh design and a huge calculation time. Moreover, the approximation of slope as rectangular steps in the two-dimensional TM mode case will have an inherent calculation error due to the fictitious charge buildup at the vertical resistivity boundary between ocean and crust. Alternatively, Baba and Seama (2002) transformed electrical conductivity and magnetic permeability

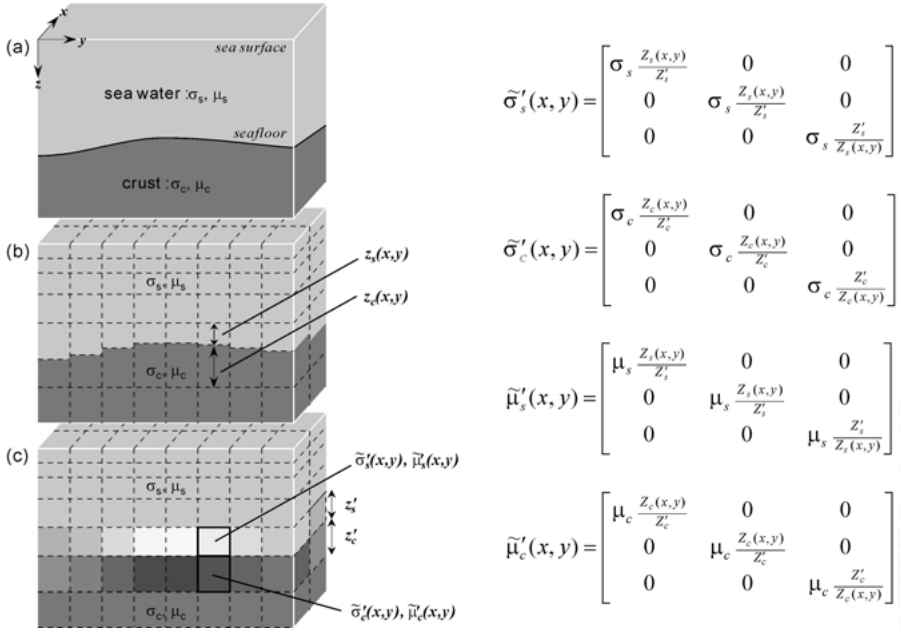

$$\tilde{\sigma}'_s(x,y)=\begin{bmatrix}\sigma_s\frac{Z_s(x,y)}{Z'_s} & 0 & 0\\ 0 & \sigma_s\frac{Z_s(x,y)}{Z'_s} & 0\\ 0 & 0 & \sigma_s\frac{Z'_s}{Z_s(x,y)}\end{bmatrix}$$

$$\tilde{\sigma}'_c(x,y)=\begin{bmatrix}\sigma_c\frac{Z_c(x,y)}{Z'_c} & 0 & 0\\ 0 & \sigma_c\frac{Z_c(x,y)}{Z'_c} & 0\\ 0 & 0 & \sigma_c\frac{Z'_c}{Z_c(x,y)}\end{bmatrix}$$

$$\tilde{\mu}'_s(x,y)=\begin{bmatrix}\mu_s\frac{Z_s(x,y)}{Z'_s} & 0 & 0\\ 0 & \mu_s\frac{Z_s(x,y)}{Z'_s} & 0\\ 0 & 0 & \mu_s\frac{Z'_s}{Z_s(x,y)}\end{bmatrix}$$

$$\tilde{\mu}'_c(x,y)=\begin{bmatrix}\mu_c\frac{Z_c(x,y)}{Z'_c} & 0 & 0\\ 0 & \mu_c\frac{Z_c(x,y)}{Z'_c} & 0\\ 0 & 0 & \mu_c\frac{Z'_c}{Z_c(x,y)}\end{bmatrix}$$

Figure 2. Effective bathymetry modeling (Baba and Seama, 2002).

so that electric and magnetic fields are calculated in evenly spaced sparse cells (Figure 2c). This transformation is based on the basic equations of Madden and Mackie (1989).

Suppose the following Maxwell's equations in a coordinate system (x_1, x_2, x_3), where μ and σ are 3×3 diagonal tensors of magnetic permeability and electrical conductivity, respectively.

$$\nabla \times E = -\mu \frac{\partial H}{\partial t},$$

$$\nabla \times H = \sigma E.$$

Then let us transform the coordinate system to a new one (x'_1, x'_2, x'_3), where $x_i = a_i x'_i$. The tensor expressions of the above formulae for i-component are as follows:

$$\epsilon_{ijk} \frac{\partial E_k}{\partial x_j} = -\mu_{ii} \frac{\partial H_i}{\partial t},$$

$$\epsilon_{ijk} \frac{\partial H_k}{\partial x_j} = \sigma_{ii} E_i.$$

By replacing $x_i = a_i x_i'$ and multiply $a_1 a_2 a_3 / a_i$, we get the followings.

$$\epsilon_{ijk} \frac{\partial (a_k E_k)}{\partial x_j'} = -\left(\mu_{ii} \frac{a_1 a_2 a_3}{a_i^2} \right) \frac{\partial (a_i H_i)}{\partial t},$$

$$\epsilon_{ijk} \frac{\partial (a_k H_k)}{\partial x_j} = \left(\sigma_{ii} \frac{a_1 a_2 a_3}{a_i^2} \right) (a_i E_i).$$

Then the corresponding electric and magnetic fields (E' and H') and magnetic permeability (μ') and electrical conductivity (σ') will be written as follows:

$$E_k' = a_k E_k, \qquad H_k' = a_k H_k,$$

$$\mu_{ii}' = \mu_{ii} \frac{a_1 a_2 a_3}{a_i^2}, \qquad \sigma_{ii}' = \sigma_{ii} \frac{a_1 a_2 a_3}{a_i^2}.$$

In the case of Baba and Seama (2002), $a_1 = a_2 = 1$ and there is only scaling for a_3. Thus the horizontal electric and magnetic fields are not affected by this scaling. The transformation was applied individually to the cells just under and over sea floor. This scheme was tested for its accuracy for two-dimensional cases. The idea can be easily applied for general three-dimensional cases.

2.5. 3D/3D MODELING

The application of Groom-Bailey decomposition is popular, but is limited to a 3D/2D case (i.e., local three-dimensional structure over regional two-dimensional structure). We can limit the use of our data in an area and period band where 3D/2D holds. In general, however, real data is often more complicated.

Ledo et al. (1998) proposed the three-dimensional galvanic distortion model over three-dimensional regional structure (3D/3D). Exactly speaking, this procedure assumes 3D/2D/3D structure (shallow 3D anomaly underlain by a 2D structure and further underlain by regional 3D structure). First of all, they use only short periods where the Groom–Bailey model holds and determine the distortion parameters. Then the same distortion parameters were used to construct twist and shear tensor for the whole period range, where the regional impedance is not necessarily off-diagonal but is a 2×2 full tensor. Then the observed impedance tensor for the whole period range is decomposed using the twist and shear determined in the short period. A full 2×2 impedance will be obtained which represents the three-dimensional regional structure.

Utada and Munekane (2000) presented 3D/3D distortion modeling using geomagnetic transfer function and arrays of MT impedances. They used the relationship between the magnetic transfer function and the spatial derivative of undistorted impedances. From Faraday's law we get the following equation for the Hz component and the regional (undistorted) electric field E.

$$-i\omega\mu H_z = \nabla \times E|_z.$$

Replacing E by $E = ZH$, we can relate magnetic transfer function to spatial derivatives of impedances. If we ignore the spatial derivative of the magnetic field and assume that magnetic distortion is negligible, the following simple relation is obtained.

$$H_z \approx A' H_x + B' H_y,$$

$$A' = \frac{i}{\omega\mu}\left[\frac{\partial Z_{yx}}{\partial x} - \frac{\partial Z_{xx}}{\partial y}\right],$$

$$B' = \frac{i}{\omega\mu}\left[\frac{\partial Z_{yy}}{\partial x} - \frac{\partial Z_{xy}}{\partial y}\right].$$

This means that the spatial gradient of the regional impedance Z should be consistent with the magnetic transfer functions. The above impedance tensor Z is a regional (distortion-removed) impedance which is related to the observed impedance Z_{obs} by a 2×2 full real tensor C as follows:

$$Z = C^{-1} Z_{\text{obs}}.$$

We can estimate the tensor C by minimizing the misfit between the observed magnetic transfer functions and impedance derived transfer function (A' and B'). This scheme needs an external control on the absolute of impedance tensors, because the magnetic transfer functions only constrain the spatial derivatives of the impedances, as seen above. Utada and Munekane(2000) successfully tested this scheme using a numerical example. Application of this technique to the real field data demands good quality in magnetic transfer functions.

3. Checking Dimensionality of the Dataset

To check the dimensionality of the dataset, physical parameters should be used which are free from near-surface distortion. A conventional way is to map induction vectors for different periods. Another way is to plot the strike estimates from decomposition. Figure 3 shows the histograms of strikes estimates for Papua New Guinea dataset (Ogawa, 1997; Jones and Schultz, 1997). Each subplot shows a histogram of strike estimates for each decade of frequency, where strike is estimated as a frequency-dependent and site-dependent parameter in a Groom–Bailey decomposition. Note that the 90 degrees ambiguity is taken into consideration. At short periods ($<$1 s), the strike estimates scatter, reflecting a contribution from shallow local structure. At longer periods, there is a consistent strike direction for the dataset. We also note the period dependence of strike directions. The deeper structure has counter-clockwise rotation relative to the shallow structure.

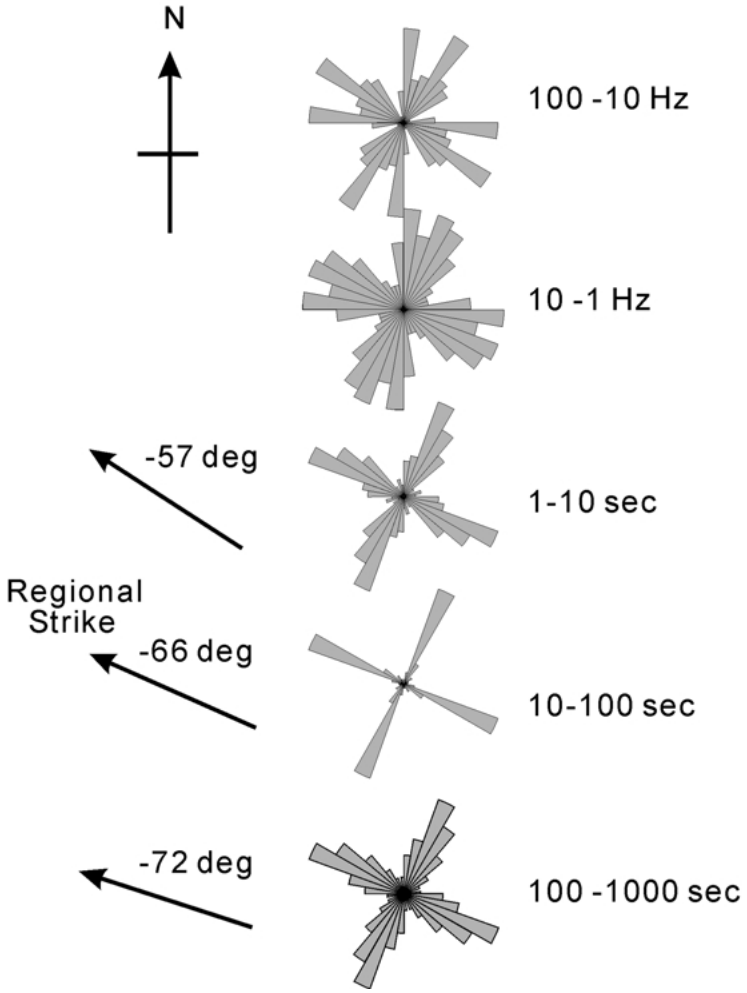

Figure 3. Rose diagrams of strikes estimates for the Papua New Guinea dataset (Ogawa, 1997).

Mapping the estimated strikes from Groom–Bailey decomposition helps the recognition of regional directional properties easily (Ogawa et al., 1994; Marquis et al., 1995; Unsworth et al., 1999). Figure 4 shows the estimated strike directions for the San Andreas Fault region for four decades of frequencies (Unsworth et al., 1999). The strike estimates between 0.1 and 10 Hz are fairly consistent with the surface trace of the San Andreas Fault. The strike significantly deviates from the fault direction below 0.1Hz, reflecting the regional effect surrounding the survey area.

For testing two-dimensionality in detail, the chi-square misfit of the data must be measured. Figure 5 shows the normalized rms misfit for a site in San Andreas Region (Unsworth et al., 1999). Increasing misfit below 0.1 Hz suggests the break-

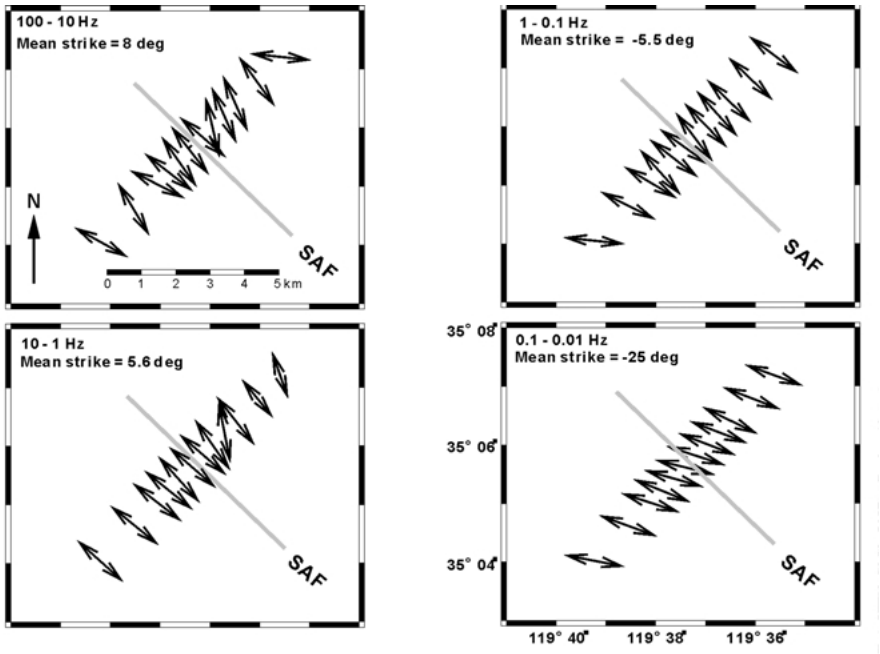

Figure 4. Regional strike estimates across the San Andreas Fault at each site for each decade of frequencies (Unsworth et al., 1999).

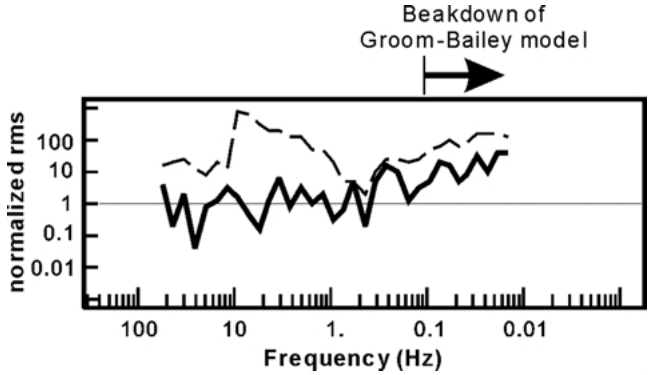

Figure 5. Misfit of the Groom-Bailey model at site 30 in the Figure 4 (Unsworth et al., 1999). The solid and dashed curves represent rms for best and worst fit while regional strike is scanned between 0 and 90 degrees.

down of Groom–Bailey decomposition, which comes from the contribution from regional three-dimensional structure. This is consistent with the strike direction in Figures 4, where a regional deviation of strike is observed below 0.1 Hz. A proper estimate of model fit and two-dimensionality requires proper estimate of errors in impedances (Chave and Jones, 1997).

4. Two-Dimensional Modeling

Two-dimensional modeling is popular and recently two-dimensional inversion is routinely applied. Here some topics on two-dimensional modeling are briefly reviewed.

4.1. Fast inversion method

The fast and stable two-dimensional inversion methods have been developed since the late 1980s and are now commonly used.

Fast calculation of the derivatives is one of the key elements in the inversion. By use of reciprocity, the partial derivatives of response functions at an observation site can be calculated by a forward calculation where a "source" is put on the observation site (Rodi, 1976; McGillivray et al., 1994; deLugao and Wannamaker, 1996). The number of forward calculations for the derivatives equals the number of sites, which usually is far smaller than the number of resistivity blocks. The use of conjugate gradients is more efficient as it requires only two forward calculations (Mackie and Madden, 1993; Rodi and Mackie, 2001) for derivatives.

The computation time can be shortened by use of approximate calculation of the partial derivatives. Approximate Inverse Mapping (AIM) (Oldenburg and Ellis, 1991) uses partial derivatives for the 1D Earth. The rapid relaxation inverse (RRI) method (Smith and Booker, 1991) fixes the horizontal derivative for iterations and inverts the structure beneath the site in a one-dimensional way. The approximation of the partial derivatives by analytic values for a uniform Earth can give enough accuracy for inversion, leading to significant time-saving (Farquharson and Oldenburg, 1996; Sasaki, 1999).

Siripunvaraporn and Egbert (2000) utilized redundancy of the electromagnetic data and developed fast codes called REBOCC. They interpolate response functions and their derivatives in the frequency-space domain.

4.2. Constraints

Model constraints are important to incorporate a priori information as well as to stabilize the inversion. Minimizing misfit alone leads to unnecessary complex structure. Penalized inversion with model roughness is widely used (Smith and Booker, 1991; deGroot-Hedlin and Constable, 1990; Uchida, 1993). Smith et al. (1999) incorporated a sharp sub-horizontal boundary in the resistivity model (Figure 6a). They demonstrated that a sharp boundary inversion clearly detects the top of the conductive layer (bottom of the resistive volcanic cover), whereas the conventional minimum structure inversion (Figure 6b) suffers from small noisy features, some of which are due to Gibbs phenomena when representing a sharp feature by a summation of smooth features. Although the penalized inversion looks objective, the choice of the constraints is not. The proper choice depends on the geologic situation of dataset.

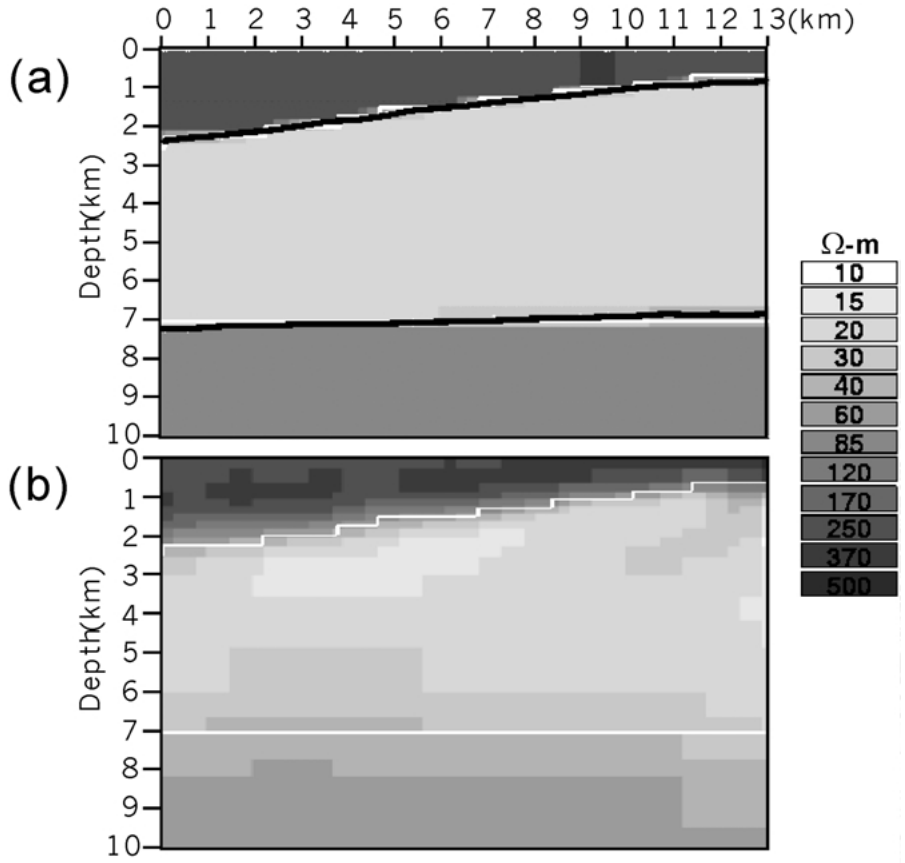

Figure 6. Effect of different constraints on the resulting models (Smith et al., 1999). (a) Sharp boundary inversion, where a three-layered structure is assumed underneath each site and the depth of the layer boundary varies smoothly. (b) Minimum structure inversion, where the Laplacian norm of the roughness is used.

Portniaguine and Zhdanov (1999) also proposed a sharp inversion algorithm where strong variation of model parameter is allowed. Their constraint is called a minimum gradient support functional, which minimize the total area with non-zero gradient of model parameters and allows large discontinuities.

Finding a proper trade-off between misfit and constraints is important. One way is to give the trade-off parameters a priori and the other is to optimize them using objective criteria such as Occam (deGroot-Hedlin and Constable, 1990) or ABIC (Uchida 1993; Ogawa and Uchida, 1996).

4.3. Limits of two-dimensional modeling

In general, the dataset shows three-dimensionality. Thus the application of a two-dimensional inversion has limits on the modes, period range and spatial range.

There is a paradigm for the use of the TM mode in a three-dimensional environment (Ting and Hohmann, 1981; Wannamaker et al., 1984, 1991). If the anomalous structure has a finite strike length, the longitudinal (electric field parallel to the structure) response differs significantly from a 2D-TE mode response, whereas the transverse response (electric field perpendicular to the structure) is similar to a 2D-TM response. This was studied for a case where a conductive anomaly is embedded in a layered Earth. The transverse response is governed by galvanic charge on the resistivity boundary similar to the case for the two-dimensional TM mode. In the case of a resistive block, however, the situation is different as the currents flows around the anomaly (Berdichevsky et al., 1998; Berdichevsky, 1999). Thus, it depends on the situation, whether the transverse mode should be emphasized as TM mode in the two-dimensional modeling.

Applicability of two-dimensional modeling can be diagnosed by use of three-dimensional forward modeling. Park and Mackie (1997) made three-dimensional modeling where exposed basement is surrounded by a conductive sedimentary basin whose strike direction is almost perpendicular to that of the regional deep structure. They showed that two dimensional modeling is usable but the use of modes is restricted in period and space.

The inclusion of surrounding area in modeling is important. Unsworth et al. (1999) report that the inclusion of regional structure outside the data area was essential in getting reasonable data fit. Figures 7 and 8 demonstrate the importance of structures outside of the profile (after Takakura, personal communication). Figure 7a is a model with a vertical conductor beneath the center of the MT profile and a lateral shallow conductor to the right of the profile. Figures 7b, c, d show the inversion results from TM only, TE only and both, respectively. In the inversion, the resistivity values of outside blocks are also variables. We note, in particular, that the TM only case (Figure 7b) has introduced a fake resistive basement below the sites. This is due to the negative sensitivity to the side structures in TM mode, i.e., the decreasing resistivity of the side block will increase the apparent resistivity of the site. Use of the TE mode (Figure 7c, d) significantly improves the inversion result. Figures 8 show similar results, but with the resistivity of the outside conductor fixed a priori before inversions. We notice the significant improvements for TM modes, by comparing Figures 7b and 8b.

4.4. Anisotropy of resistivity structure

We often have different responses in TE and TM modes. These are “anisotropic responses” in the magnetotelluric impedances. One way to interpret these is to make a resistivity model that consists of many blocks of isotropic resistivity. The other way is to have some blocks of “anisotropic resistivity”, where resistivity depends on the directions. Anisotropy (anisotropy of resistivity structure) has been an interesting topic in recent years (e.g., Mareschal et al., 1995; Eisel and Haak, 1999).

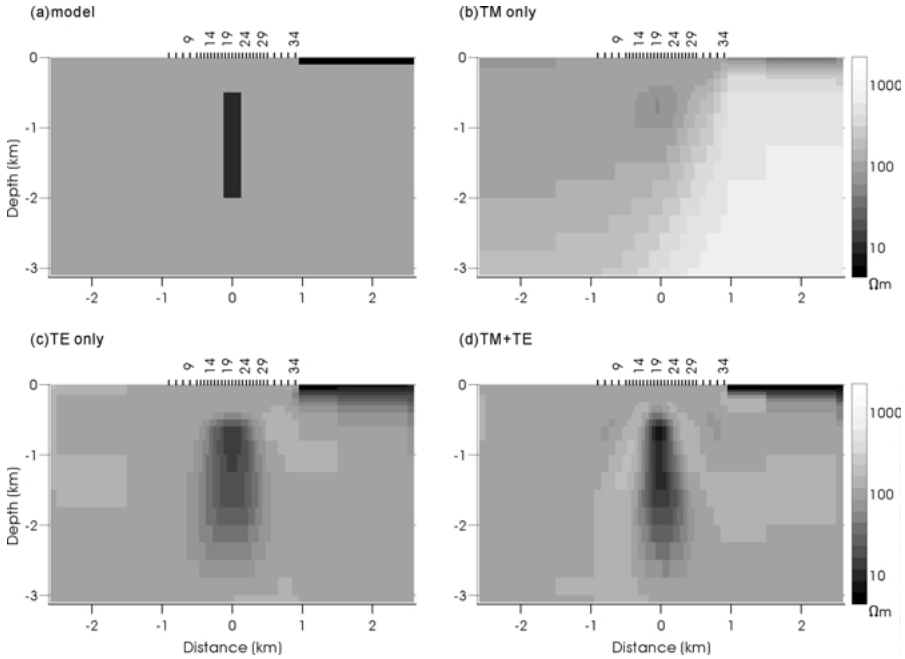

Figure 7. Effect of outside structure on two-dimensional inversion using minimum structure constraint (after Takakura, personal communication). (a) True model. Ticks on the surface denote magnetotelluric sites. (b) Inversion result of TM data with 3% noise added. (c) Inversion result of TE data with 3% noise added (d) Inversion of both TM and TE data with 3% noise. These inversions do not account for the shallow conductive anomaly a priori to the right of the profile.

In usual magnetotellurics, the electric current flows predominantly horizontally. Thus the horizontal anisotropy is emphasized. The most simple case is a two-dimensional vertical structure where multiple conductive vertical dikes (conductivity σ_1) exist in a resistive host (σ_2). In case of TE mode, the current will flow more along the conductive dyke, the resistors are connected in parallel and σ_1 will dominate the response. On the other hand, in the TM mode, the current flows across the resistivity contact, and the resistors are connected in serial and σ_2 dominates. Then, in many cases TE and TM mode responses require conductor and resistor, respectively.

Eisel and Haak (1999) showed two resistivity models to explain anisotropic response of the KTB region (Figure 9). One model (Figure 9a) is an intrinsic anisotropy model, where particular blocks have anisotropy in TE/TM modes. The other is a regional anisotropy model (Figure 9b) with sub-vertical thin conductors which are only sensed in the TE mode. These two models show non-uniqueness of the anisotropy modeling.

Two-dimensional models usually have anisotropic response, of course. If we invert each mode separately, we have two different resistivity structures (for example Figures 7b and 7c). This difference in modes is due to different sensitivity

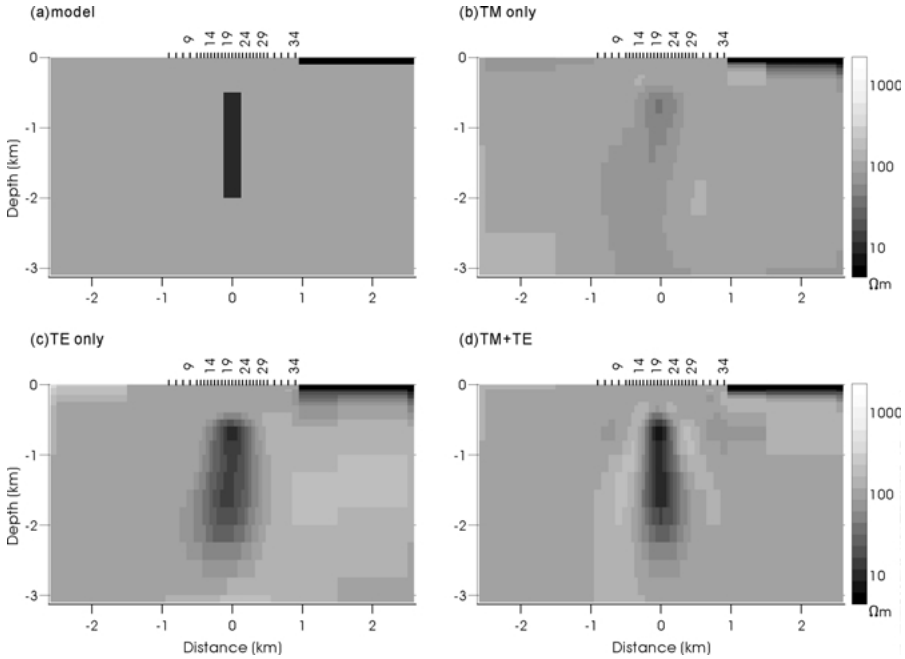

Figure 8. Same as Figure 7 except that the shallow structure to the right of site 34 is accounted for during inversions (after Takakura, personal communication).

to complex structures and does not always support anisotropy. Thus the introduction of an anisotropic block is not always required in general. In the case of Mareschal et al. (1995), a null transfer function was the supporting evidence for the anisotropic mantle. They insisted that the anisotropic responses are not due to lateral heterogeneity, but rather due to intrinsic anisotropy. In case there are lateral inhomogeneities, the separation of lateral resistivity variations and the intrinsic anisotropy is difficult. Alternatively other geological or geophysical information will support the existence of anisotropy (e.g., Mareschal et al., 1995; Jones et al., 1997; Eisel and Haak, 1999).

Most anisotropy modeling has the anisotropy axes along and perpendicular to the two-dimensional coordinate frame. Pek and Verner (1997) made anisotropy modeling for a more general anisotropy case, where TE and TM modes are coupled.

5. Three-Dimensional Modeling of the Field Dataset and Future Work

Recent advances in equipments make the deployment of many sites feasible. Three-dimensional modeling has started for field datasets. In case of spatially sparse magnetotelluric data, control of the surface resistivity distribution is important. If we can assume good correlation of resistivity with another surface geophysical

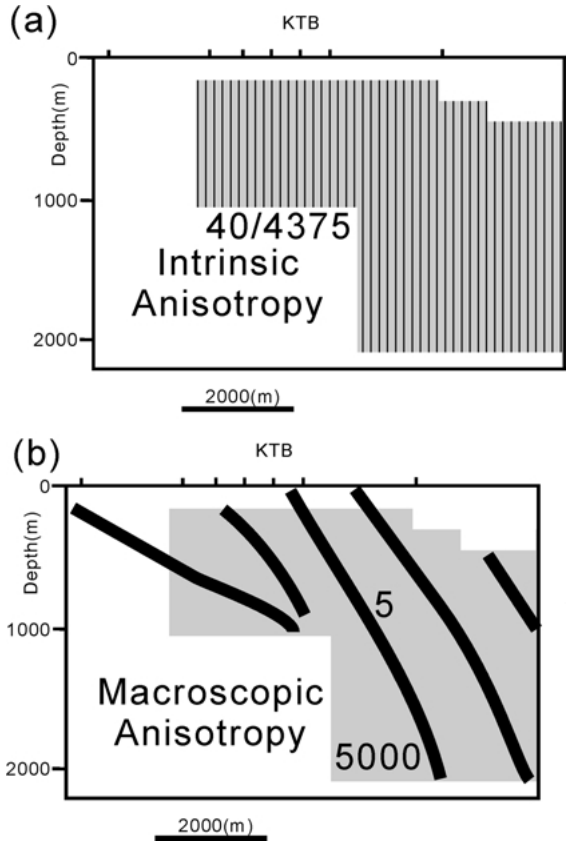

Figure 9. Two anisotropic models (Eisel and Haak, 1999) (a) Intrinsic anisotropy model where the anomalous block shows 40 Ωm and 4375 Ωm for TE and TM mode respectively. (b) Macroscopic anisotropy model, where the host block shows generally high resistivity (5,000 Ωm) and the multiple fracture zones have low resistivity (5 Ωm).

parameters, we can use them to control the surface regional structures. Pous et al. (1995) used gravity basement for controlling the regional surface of sedimentary layer as constraints for regional three-dimensional modeling.

3D inversions for field data have been reported recently. Matsuo and Negi (1999) inverted a 3D-MT dataset in Japan for petroleum exploration. They used the quasi-linear approximation code of Zhdanov and Fang (1995). Uchida et al. (2000) applied the three-dimensional inversion code of Sasaki (1999) for geothermal exploration dataset in Indonesia. The two inversion results from two different choices of coordinate frames (one is rotated 45 degrees from the other) were almost identical, showing the effectiveness of the modeling scheme.

These pioneer works, however, lack in handling the near surface distortions. In these cases, the static effect may be realized by a resistivity contrast of neighboring surface blocks, although the real cause may be of much smaller origin. Phase mix-

ing is more difficult to explain by near-surface blocks, as its realization probably needs much finer structures than the target structure. The modeling needs removal of galvanic distortion beforehand similar to the two-dimensional case. Joint inversion of galvanic distortion and three-dimensional modeling will be a good alternative, as was demonstrated by deGroot-Hedlin (1995) for two-dimensional case.

Use of constraints will be important for three-dimensional inversion in order to incorporate a priori information and to stabilize the inversion. In order to investigate deep crustal structures, we can use other geophysical parameters to constrain the shallow structure, if we can assume strong correlations between resistivity and other geophysical parameters. Finding proper trade-off parameters between data misfit and norms of constraints will also be important.

Acknowledgement

I would like to thank the IAGA working group 1.2 for providing me an opportunity to present this review paper at the 15th Electromagnetic Induction Workshop at Cabo Frio, Brazil. I acknowledge Hiroshi Munekane, Kiyoshi Baba, Martyn Unsworth, Torquil Smith and Shinichi Takakura who provided me the original figures. The reviews by three anonymous referees significantly improved the manuscript. The citations of the previous publications in this paper depend on my ability and do not cover all the relevant literatures.

References

Agarwal, A.K. and Weaver, J.T.: 2000, Magnetic distortion of the magnetotelluric tensor: a numerical study, *Earth Planets Space* **52**, 347–353.

Baba, K. and Seama, N.: 2002, A new technique for the incorporation of seafloor topography in electromagnetic modeling, submitted to *Geophys. J. Internat*., in press.

Bahr, K.: 1985, Interpretation of the magnetotelluric impedance tensor: regional induction and local telluric distortion, *J. Geophys.* **62**, 119–127.

Berdichevsky, M.N, Dmitriev, V.I., and Pozdnjakova, E.E.: 1998, On two-dimensional interpretation of magnetotelluric soundings, *Geophys. J. Internat.* **133**, 585–606.

Berdichevsky, M.N. and Dmitriev, V.I.: 1976, Distortion of magnetic and electric fields by near surface lateral inhomogeneities, *Acta Geidat. Geophys. Et Montanist. Acad. Sci. Hung.* **11**, 447–483.

Berdichevsky, M.N., Vanyan, L.L., Kuznetsov, V.A., Levadny, V.T., Mandelbaum, M.M., Nechaeva, G.P., Okulessky, B.A., Shilovsky, P.P., and Shpak, I.P.: 1980, *Geoelectrical model of the Bikal region, Phys. Earth Planet. Inter.* **22**, 1–11.

Berdichevsky, M.N.: 1999, Marginal notes on magnetotellurics, *Surveys in Geophysics* **20**(3–4), 341–375.

Chave, A.D. and Smith, J.T.: 1994, On electric and magnetic galvanic distortion tensor decomposition, *J. Geophys. Res.* **99**, 4669–4682.

Chave, A.D. and Thomson, D.J.: 1989, Some comments on magnetotellurics response function estimation, *J. Geophys. Res.* **94**, 14,215–14,225.

Chave, A.D. and Jones, A.G.: 1997, Electric and magnetic field distortion decomposition of BC87 data, *J. Geomagn. Geoelectr.* **49**, 767–789.

deGroot-Hedlin, C. and Constable, S.: 1990, Occam inversion to create smooth 2-dimensional models from magnetotelluric data, *Geophysics* **55**, 1613–1624.

deGroot-Hedlin, C.: 1991, Removal of static shift in 2-dimensions by regularized inversion, *Geophysics* **56**, 2102–2106.

deGroot-Hedlin, C.: 1995, Inversion for regional 2-d resistivity structure in the presence of galvanic scatterers, *Geophys. J. Internat.* **122**(3), 877–888.

deLugao, P.P., Wannamaker, P.E.: 1996, Calculating the two-dimensional magnetotelluric Jacobian in finite elements using reciprocity, *Geophys. J. Int.* **127**, 806–810.

Egbert, G.D.: 1997, Robust multiple-station magnetotelluric data processing, *Geophys. J. Internat.* **130**, 475–496.

Eisel, M. and Haak, V.: 1999, Macro-anisotropy of the electrical conductivity of the crust: a magnetotelluric study of the German Continental Deep Drilling site (KTB), *Geophys. J. Internat.* **136**, 109–122.

Farquharson, C.G. and Oldenburg, D.W.: 1996, Approximate sensitivities for the electromagnetic inverse problems, *Geophys. J. Internat.* **126**, 235–252.

Groom, R.W. and Bailey, R.C.: 1989, Decomposition of magnetotellurics impedance tensors in the presence of local three-dimensional galvanic distortions, *J. Geophys. Res.* **94**, 1913–1925.

Harinarayana, T.: 1999, Combination of EM and DC measurements for upper crustal studies, *Surveys in Geophysics* **20**, 257–278.

Jiracek, G.R., Redding, R.P., and Kojima, R.K.: 1989, Application of the Rayleigh-FFT technique to magnetotelluric modeling and correction, *Phys. Earth Planet. Inter.* **53**, 365–375.

Jiracek, G.R.: 1990, Near-surface and topographic distortions in electromagnetic induction, *Surveys in Geophysics* **11**, 163–203.

Jones, A.G., Gough, D.I., Kurtz, R.D., DeLaurier, J.M., Boerner, D.E., Craven, J.A., Ellis, R.G., and McNeice, G.W.: 1992, Electromagnetic images of regional structure in the southern Cordillera, *Geophys. Res. Lett.* **12**, 2373–2376.

Jones, A.G.: 1988, Static shift of magnetotelluric data and its removal in a sedimentary basin environment, *Geophysics* **53**, 967–978.

Jones, A.G.: 1993, The COPROD2 dataset – Tectonic setting, recorded MT data, and comparison of models, *J. Geomag. Geoelectr.* **45**, 933–955.

Jones, A.G. and Groom, R.W.: 1993, Strike angle determination from the magnetotelluric tensor in the presence of noise and local distortion: rotate at your peril!, *Geophys. J. Internat.* **113**, 524–534.

Jones, A.G. and Schultz, A.: 1997, Introduction to MT-DIW2 Special Issue, *J. Geomag. Geoelectr.* **49**, 727–737.

Jones, A.G., Katsube, T.J., and Schwann, P.: 1997, The longest conductivity anomaly in the world explained: sulphides in fold hinges causing very high electrical anisotropy, *J. Geomag. Geoelectr.* **49**, 1619–1629.

Larsen, J.C., Mackie, R.L., Manzella, A., Fiordelisi, A., and Rieven, S.: 1996, Robust smooth magnetotelluric transfer functions, *Geophys. J. Internat.* **124**, 801–819.

Larsen, J.C.: 1977, Removal of local surface conductivity effects from low frequency mantle response curves, *Acta Geodaet. Geophys.Acad. Sci. Hung.* **12**, 183–186.

Ledo, J, Queralt, P, and Pous, J: 1998, Effects of galvanic distortion on magnetotelluric data over a three-dimensional regional structure, *Geophys. J. Internat.* **132**, 295–301.

Mackie, R.L. and Madden, T.R.: 1993, Three-dimensional Magnetotelluric inversion using conjugate gradients, *Geophys. J. Internat.* **115**, 215–229.

Madden, T.R. and Mackie, R.L.: 1989. Three-dimensional magnetotellurics modeling and inversion, *Proc. IEEE* **77**, 318–333.

Mareschal, M., Kellett, R.L., Kurtz, R.D., Ludden, J.N., Ji, S., and Bailey, R.C.: 1995, Archean cratonic roots, mantle shear and deep electrical anisotropy, *Nature* **375**, 134–137.

Marquis, G., Jones, A.G., and Hyndman, R.D.: 1995, Coincident conductive and reflective middle and lower crust in southern British Columbia, *Geophys. J. Internal.* **120**, 111–131.

Matsuo, K. and Negi, T.: 1999, Oil exploration in the difficult Minami-Noshiro area, Part 2, magnetotelluric survey, the leading edge, **18**, 1411–1413.

McGillivray, P.R., Oldenburg, D.W., Ellis, R.G., and Habashy, T.M.: 1994, Calculation of sensitivities for the frequency-domain electromagnetic problem, *Geophys. J. Internat.* **116**, 1–4.

McNeice, G.W. and Jones, A.G.: 2001, Multi-site, multi-frequency tensor decomposition of magnetotelluric data, *Geophysics* **66**, 158–163.

Meju, M.A.: 1996, Joint inversion of TEM and distorted MT soundings: Some effective practical considerations, *Geophysics* **61**, 56–65.

Nolasco, R., Tarits, P., Filloux, J.H., and Chave, A.D.: 1998, Magnetotelluric imaging of the Society Islands hotspot, *J. Geophys. Res.* **103**, 30287–30309.

Ogawa, Y., Nishida,Y., and Makino, M.: 1994, A collision boundary imaged by magnetotellurics, Hidaka Mountains, central Hokkaido, Japan, *J. Geophys. Res.* **99**, 22373–22388.

Ogawa, Y. and Uchida, T.: 1996, A two-dimensional magnetotelluric inversion assuming Gaussian static shift, *Geophys. J. Internat.* **126**, 69–76.

Ogawa, Y., 1997: Two-dimensional inversion of Papua New Guinea magnetotellurics dataset assuming static shift as Gaussian distribution, *J. Geomag. Geoelectr.* **49**, 857–867.

Ogawa, Y., Matsushima, N., Oshima, H., Takakura, S., Utsugi, M., Hirano, K., Igarashi, M., and Doi, T.: 1998, A resistivity cross-section of Usu volcano, Hokkaido, Japan, by audiomagnetotellurics soundings, *Earth Planets Space* **50**, 339–346.

Ogawa, Y.: 1999, Constrained inversion of COPROD-2S2 dataset using model roughness and static shift norm, *Earth Planets Space* **51**, 1145–1151.

Oldenburg, D.W. and Ellis, R.G.: 1991, Inversion of geophysical data using approximate inverse mapping, *Geophys. J. Internat.* **105**, 325–353.

Park, S.K. and Mackie, R.J.: 1997, Crustal structure at Nanga Parbat, Northern Pakistan, from magnetotelluric soundings, *Geophys. Res. Lett.* **24**, 2415–2418.

Pek, J. and Verner, T.: 1997, Finite-difference modeling of magnetotelluric fields in two-dimensional anisotropic media, *Geophys. J. Internat.* **128**, 505–521.

Pellerin, L. and Hohmann, G.W.: 1990, Transient electromagnetic inversion – a remedy for magnetotelluric static shifts, *Geophysics* **55**, 1242–1250.

Pous, J., Ayala, C., Ledo, J., Marcuello, A., and Sabat, F.: 1995, 3D modeling of magnetotelluric and gravity data of Mallorca island (Western Mediterranean), *Geophys. Res. Lett.* **22**, 735–738.

Portniaguine, O. and Zhdanov, M.S.: 1999, Focusing geophysical inversion images, *Geophysics* **64**, 874–887.

Rodi, W.L. and Mackie, R.L.: 2001, Nonlinear conjugate gradients algorithm for 2-D magnetotelluric inversion, *Geophysics* **66**, 174–187.

Rodi, W.L.: 1976, A technique for improving the accuracy of finite element solutions for Magnetotelluric data, *Geophys. J. R.astro. Soc.* **44**, 483–506, 1976.

Sasaki, Y.: 1999, 3D inversion of electrical and electromagnetic data on PC, the second international symposium on three-dimensional electromagnetics (3DEM-2), the University of Utah, 128–131.

Schultz, A., Kurtz, R.D., Chave A.D., and Jones, A.G.: 1993, Conductivity discontinuities in the upper mantle beneath a stable craton, *Geophys. Res. Lett.* **20**, 2941–2944.

Siripunvaraporn, W. and Egbert, G.: 2000, An efficient data-subspace inversion method for 2-D Magnetotelluric data, *Geophysics* **65**, 791–803.

Smith, J.T. and Booker, J.R.: 1991, Rapid inversion of two- and three-dimensional magnetotelluric data, *J. Geophys, Res.* **96**, 3905–3922.

Smith, J.T.: 1995, Understanding telluric distortion matrices, *Geophys. J. Internat.* **122**, 219–226. Smith, J.T.: 1997, Estimating galvanic-distortion magnetic fields in magnetotellurics, *Geophys. J. Internat.* **130**, 65–72.

Smith, T., Hoversten, M., Gasperikova, E., and Morrison, F.: 1999, Sharp boundary inversion of 2D magnetotelluric data, *Geophys. Prospecting* **47**, 469–486.

Ting, S.C. and Hohmann, G.W.: 1981, Integral equation modeling of three-dimensional magnetotelluric response, *Geophysics* **46**, 192–197.

Torres-Verdin, C. and Bostick, F.X.: 1992, Principles of spatial surface electric-field filtering in magnetotellurics – electromagnetic array profiling (EMAP), *Geophysics* **57**, 603–622.

Tournerie, B. and Chouteau, M.: 1998, Deep conductivity structure in Abitibi, Canada, using long dipole magnetotelluric measurements, *Geophys. Res. Lett.* **25**, 2317–2320.

Uchida, T., Honda, M., Ashari, and Andan, A.: 2000, Magnetotelluric investigation at the Bajawa geothermal field in Flores Island, Eastern Indonesia, presented at 15th EM Induction Workshop.

Uchida, T.: 1993, Smooth 2-D inversion of Magnetotelluric data based on statistical criterion ABIC, *J.Geomag.Geoelectr.* **45**, 841–858.

Unsworth, M.J., Egbert, G., and Booker, J.R.: 1999, High-resolution electromagnetic imaging of the San Andreas fault in central California, *J. Geophys. Res.* **104**, 1131–1150.

Utada, H. and Munekane, H.: 2000, On galvanic distortion of regional three-dimensional magnetotelluric impedances, *Geophys. J. Internat.* **140**, 385–398.

Uyeshima, M., Utada, H., and Nishida, Y.: 2001, Network-magnetotelluric method and its first results in central and eastern Hokkaido, NE, Japan, *Geophys. J. Internat.* **146**, 1–19.

Wannamaker, P.E., Stodt, J.A., and Rijo, L.: 1986, Two-dimensional topographic responses in magnetotelluric model using finite elements, *Geophysics* **51**, 2131–2144.

Wannamaker, P.E., Ward, S.H., and Hohmann, G.W.: 1984, Magnetotelluric responses of three-dimensional bodies in layered Earth, *Geophysics* **49**, 1517–1533.

Wannamaker, P.E., Wright, P.M., Zhou, Z.X., Li, X.B., and Zhao, J.X.: 1991, Magnetotelluric transect of long valley caldera-resistivity cross-section, structural implications, and the limits of a 2D analysis, *Geophysics* **56**, 926–940.

White, S.N., Chave, A.D., and Filloux J.H.: 1997, A look at galvanic distortion in the Tasman Sea and the Juan de Fuca plate, *J. Geomag. Geoelectr.* **49**(11–12), 1373–1386.

Wu, N., Booker, J.R., and Smith, J.T.: 1993, Rapid two-dimensional inversion of COPROD2 data, *J. Geomag. Geoelectr.* **45**, 1073–1087.

Zhdanov, M.S. and Fang, S.: 1995, Rapid 3-d electromagnetic inversion based on quasi-linear approximation, Ann. Internat. Mtg., Soc. Expl. Geophys., Expanded abstracts, 254–257.